Hindawi
Advances in Materials Science and Engineering
Volume 2022, Article ID 2943138, 12 pages
https://doi.org/10.1155/2022/2943138

Research Article

Repeated Uniaxial Compression Test of Permeable Friction Courses Mixtures under Seepage Field and Stress Field Coupling

Zhang Xingmei,[1,2] Li Yarui,[1] and Yang Datian[1]

[1]*College of Civil Engnieering, Chongqing Jiaotong University, Chongqing 400074, China*
[2]*Chongqing Radio and TV University, Chongqing 400052, China*

Correspondence should be addressed to Yang Datian; tywoyangda@cqjtu.edu.cn

Received 23 June 2022; Revised 6 August 2022; Accepted 10 August 2022; Published 25 September 2022

Academic Editor: Chunli Wu

In order to study the variations of the non-Darcy flow permeability coefficient and the porosity of permeable friction courses (PFCs), as well as the effects of the coupled seepage and stress fields on them, repeated uniaxial compression tests were carried out under the coupled action of water and a load. A set of water and load coupling tests were conducted, and a non-Darcy flow permeability coefficient tester was also made. After the PFC-13 specimen was carried out by the repeated uniaxial compression test under the water and load coupling, the total air void ratio and effective air void ratio were measured by the vacuum sealing method, and the non-Darcy flow permeability coefficients were obtained by a non-Darcy flow permeability coefficient tester. It was found that the coupled action of water and a load caused the total air void ratio, effective air void ratio, and permeability coefficient to sharply increase and reduced the number of repeated uniaxial compression cycles. These results are helpful for the design, construction, and maintenance of PFC mixtures.

1. Introduction

Permeable friction courses (PFCs) [1] are a new generation of open-graded friction courses (OGFCs). PFCs typically contain at least 20% more asphalt binder (by volume) than conventional OGFC mixtures. PFCs contain 18%–22% air voids, whereas conventional OGFC mixtures only contain 10%–15% air voids [2]. Unlike conventional OGFCs, PFCs typically contain polymer fibers [1].

PFCs have many advantages, but durability is a critical issue. The existing standard methods to evaluate the durability of PFCs typically only include the Cantabro loss [3, 4], the indirect tensile (IDT) strength [3, 4], and the Hamburg wheel tracking test (HWTT) [5].

Poulikakos et al. used a coaxial shear test and wheel tracking tests to investigate the mechanical properties of porous asphalt mixtures [6]. Because PFC mixtures have large air voids, the freeze-thaw process cannot cause internal damage, and therefore, the indirect tensile strength is less likely to decrease. At the same time, there is water in the voids, which influences the Cantabro loss in the Cantabro test. Huang et al. [7] used fracture energy to evaluate the durability of porous asphalt mixture.

The coaxial shear test and Hamburg wheel tracking test can simulate a load and the influence of water and temperature. However, water does not flow in the pores, and thus, the test cannot reflect the seepage process of rainwater in the pores. Yang and Zhou [8] investigated the immersion fatigue of a dense asphalt mixture and found that the effect of static and dynamic water on the fatigue lives of asphalt mixtures was not significant.

The main causes of asphalt pavement damage are a heavy load and repeated rolling. In addition, excess-pressure pore water is also an important factor causing asphalt pavement damage. The existence of moisture significantly affects the material properties of the asphalt mixture, and it changes the mechanical response of the asphalt mixture under a load. In the process of water seepage, the change of the seepage field

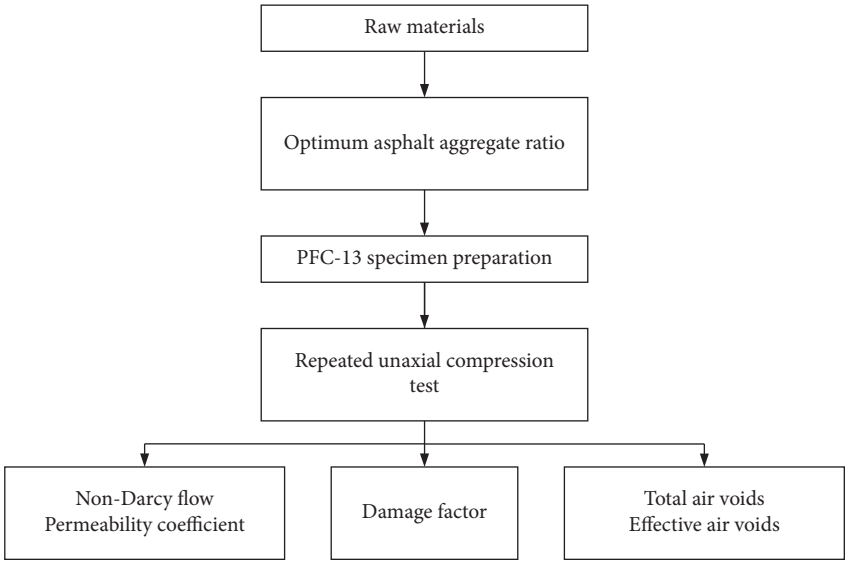

Figure 1: Flowchart of study materials and corresponding test methods.

leads to the redistribution of stress in the mixture. At the same time, due to the change in stress, the void ratio and void volume will also be affected.

Kringosn et al. [9] believed that water intruded into the gaps between the asphalt and aggregate and produced a pumping effect under a load, resulting in water damage, and they established a fluid-solid coupling model based on this. Si et al. [10] established a viscoelastic constitutive equation of asphalt and a finite element model of asphalt pavement, deduced the stress seepage coupling equation of asphalt pavement, and verified the effectiveness of the model. Ding and Wang [11] analyzed the mechanical response of saturated asphalt pavement under the coupling of a seepage field and a stress field.

Sun et al. [12] studied the dynamic response of unsaturated permeable asphalt pavement under a moving load with a three-dimensional finite element model with the coupling of water, air, and forces based on unsaturated seepage theory. Si et al. [13] computed the mechanical response of asphalt pavement under rainfall with the finite element method.

From above the papers, it was found that the variations of non-Darcy flow permeability coefficient and the porosity of permeable asphalt mixture samples, as well as the effects of the coupled seepage and stress fields on them, have been less studied after repeated uniaxial compression tests.

In this paper, first, the optimal asphalt-aggregate ratio was determined by a draindown loss test. Second, PFC-13 specimens were formed by a gyratory compactor. Water and load coupling tests were conducted, and non-Darcy flow permeability tests were also conducted. After the specimens underwent repeated uniaxial compression tests under the coupled action of water and a load, the total air void and effective air void ratios were measured by a vacuum sealing method, and the non-Darcy flow permeability coefficients were obtained by a non-Darcy flow permeability tester. The materials and corresponding test methods used in this study are summarized as a flowchart in Figure 1.

2. Materials

2.1. High-Viscosity Polymer-Modified Asphalt. The high-viscosity polymer-modified asphalt composed of a high-viscosity polymer modifier and styrene-butadiene-styrene (SBS) polymer-modified asphalt, and they were mixed together and sheared for 30 min at 4000–5000 r/min and 180°C [14]. The technical properties [15] are shown in Table 1.

2.2. Aggregate

2.2.1. Coarse Aggregate. Hard sandstone aggregate was used to form a skeleton contact structure of the coarse aggregate. The technical properties [2] are shown in Table 2.

2.2.2. Fine Aggregate. The fine aggregate used was limestone-manufactured sand. The technical properties [2] are shown in Table 3.

2.3. Filler. The filler was limestone powder, which could significantly enhance the adhesion between the aggregate particles [2]. The technical properties are shown in Table 4.

2.4. Fiber Stabilizer. Polyester fiber does not absorb water, which is helpful in improving the moisture stability of PFC mixtures. At the same time, the polyester fiber was easily dispersed during the mixing process. Hence, polyester fibers with lengths of 9 mm and diameters of 15 μm were used.

3. Aggregate Gradation and Optimal Asphalt-Aggregate Ratio

3.1. Aggregate Gradation. The 10–15 mm coarse aggregate, 0–5 mm fine aggregate, and the filler were sieved. Their results are shown in Table 5. According to the technical

Table 1: Technical properties of high-viscosity polymer-modified asphalt.

No.	Item	Unit	Requirements	Results
1	Penetration degree (25°C, 100 g, 5 s)	0.1 mm	40–60	48
2	Ductility (5°C, 5 cm/min)	cm	≥ 35	47
3	Softening point $T_{R\&B}$	°C	≥ 85	97
4	Capillary dynamic viscosity, 60°C	kPa·s	400–800	509.6
5	Viscosity, 25°C	N·m	≥ 25	53.3
6	Toughness, 25°C	N·m	≥ 20	35.0
7	Elastic recovery, 25°C	%	≥ 90	99.3

Table 2: Technical properties of hard sandstone aggregate.

No.	Item	Unit	Requirements	Results
1	Stone crushing value	%	≤ 24	9.5
2	Los Angeles abrasion loss	%	≤ 26	10.4
3	Apparent relative density	—	≥ 2.60	2.912
4	Water absorption	%	≤ 2.0	0.8
5	Robustness	%	≤ 12	1.3
6	Flatness, elongated particles	%	≤ 10	9.0
7	Particle content smaller than 0.075 mm	%	≤ 1	0.6
8	Soft stone content	%	≤ 1.0	0
9	Polishing value	PSV	≥ 42	52
10	Adhesion level for asphalt	—	Level 5	Level 5

Table 3: Technical properties of limestone machine-made sand.

No.	Items	Unit	Requirements	Results
1	Apparent relative density	—	≥ 2.60	2.912
2	Particle content smaller than 0.075 mm	%	≤ 1	0.6

Table 4: Technical properties of limestone filler.

No.	Item	Unit	Requirements	Results
1	Apparent relative density	—	≥ 2.60	2.723
2	Particle size range	—	—	—
	< 0.6 mm	%	100	100
	< 0.3 mm	%	95–100	99.8
	< 0.15 mm.	%	90–100	95.4
	< 0.075 mm	%	75–100	79.9

requirements [15], the combined aggregate gradation of PFC-13 is shown in Table 6.

3.2. Optimal Asphalt-Aggregate Ratio. First, five groups of PFC-13 mixtures were prepared according to the suggested asphalt-aggregate ratio of ±0.5%. Second, the draindown losses of the PFC-13 mixtures were measured. Finally, fitted power function curves were obtained. Two tangent lines, labeled l and m, were drawn, which intersected at point A. The straight line labeled o bisected the angle φ and intersected the fitted curve at point B. Through point B, the vertical straight line n of the horizontal axis (asphalt-stone ratio) was drawn and intersected at point D. The value corresponding to point D was the optimal asphalt-stone ratio [15], as shown in Figure 2. According to Figure 2, the optimal asphalt-aggregate ratio was 5.1%.

4. Repeated Uniaxial Compression Test of Seepage and Stress Field Coupling

A seepage field is a water flow field in which water with a certain flow velocity flows from a porous medium. If there is no other load coupled with it, the water seepage field is a hydrostatic seepage field, and hydrostatic pressure is applied to the pore walls [16]. The stress field is due to an applied external load on the top surface of the sample, which acts on the sample and generates a stress field in the porous medium. For a porous medium similar to a permeable asphalt mixture, this stress field is borne by the particle skeleton around the pores.

When a seepage field and a stress field are generated simultaneously in the porous medium, the seepage-stress coupled field is formed in the porous medium. In order to simulate the damage of the permeable asphalt mixture specimen caused by the coupling of seepage and stress fields, a system for performing repeated uniaxial compression tests under the coupling of a seepage field and a stress field was designed and fabricated, as shown in Figure 3. The water flow volume, which was coupled with the stress field, was about 5 L/h [17]. This simulated the non-Darcy flow seepage of a rainstorm in permeable asphalt mixture pavement, forming a seepage field.

As shown in Figure 3, the seepage field was established with a water pump, transparent rubber pipe, flowmeter, loading permeable plate, and water tank. The red circle

Table 5: Aggregate sieving analysis.

Aggregate size	Sieve size									
	16	13.2	9.5	4.75	2.36	1.18	0.6	0.3	0.15	0.075
	Percentage of weight passing (%)									
10–15	100.0	93.0	14.5	1.2	1.2	1.0	1.0	1.0	1.0	1.0
0–5	100.0	100.0	100.0	100.0	84.2	59.3	40.3	25.5	18.3	14.5
Filler	100.0	100.0	100.0	100.0	100.0	100.0	100.0	99.8	95.4	79.9

Table 6: Combined aggregate gradation of PFC-13.

Gradation	Percentage of weight passing (%)									
	16	13.2	9.5	4.75	2.36	1.18	0.6	0.3	0.15	0.075
Gradation two	100.0	94.1	27.3	16.0	13.9	10.6	8.1	6.2	5.2	4.4

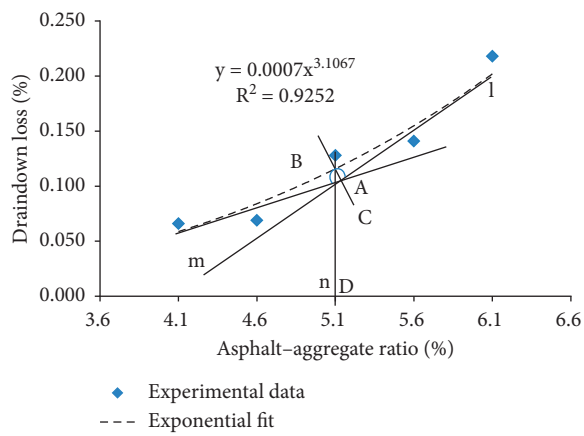

Figure 2: Draindown loss vs. asphalt-aggregate ratio.

highlights the water flowmeter. Water seeped into the permeable asphalt mixture specimen through the water flowmeter and a loading plate to simulate the seepage process of rainwater in the permeable asphalt mixture pavement. To describe the process of the seepage and stress field coupling, a schematic diagram of the coupling test is shown in Figure 4.

As shown in Figure 4, water percolated into the permeable asphalt mixture specimen at a certain flow rate, and a seepage-stress coupled field was formed in the permeable asphalt mixture specimen together with the load on the top of the specimen to jointly load the permeable asphalt mixture specimen. The impermeable metal floor simulated the impermeable layer. Water seeped out from the side wall of the permeable asphalt mixture specimen and the top part of the impermeable metal base plate.

5. Non-Darcy Flow Permeability Coefficient of Compacted Permeable Asphalt Mixture

In order to obtain the non-Darcy flow permeability coefficient (or hydraulic conductivity) of the compacted permeable asphalt mixture, a non-Darcy flow permeability tester was designed and fabricated. Its design sketch is shown in Figure 5, and Figure 6 shows a photograph of the actual system.

Based on Figure 5, the water heads at ϕ_1 and ϕ_2 can be expressed as

$$\phi_1 = z_1 + \frac{P_1}{\rho g}, \tag{1}$$

$$\phi_2 = z_2 + \frac{P_2}{\rho g}, \tag{2}$$

where Z_1 is the water head at the position of the inlet section of the sample with respect to the reference plane 0–0, Z_2 is the water head at the position of the outlet section of the sample with respect to the reference plane 0–0, P_1 is the water pressure on the inlet section of the sample, whose value is equal to the water head of the water column $\phi_1 - Z_1$, P_2 is the water pressure on the outlet section of the sample, whose value is equal to the water column $\phi_2 - Z_2$, ρ is the density of water, generally taken as 1.0×10^3 kg/m^3, and g is the gravitational acceleration, generally taken as 9.81 m/s^2.

The rate of water flow Q (volume per unit time) is equal to the product of the average seepage velocity u and the constant cross-sectional area A, i.e.,

$$u = \frac{Q}{A}, \tag{3}$$

where u is the average seepage velocity of water in the porous medium (m/s), Q is the rate of water flow (volume per unit time) through the porous medium sample (m^3/s), and A is the cross-sectional area of the porous medium sample (m^2).

Considering the effective porosity φ of the porous media sample [16], (3) is rewritten as

$$u = \varphi \frac{Q}{A}. \tag{4}$$

When water is in a laminar flow state in the porous medium, i.e., Darcy's flow, the permeability coefficient of Darcy's flow [18] is calculated through Darcy's law, as follows:

$$-\frac{\partial P}{\partial X} = \frac{1}{k}\mu u, \tag{5}$$

where P is the pressure (Pa), X is the seepage length of water in the porous medium (m), μ is the dynamic viscosity (the dynamic viscosity of water is 1.01×10^{-3} Pa s at 20°C), u is the

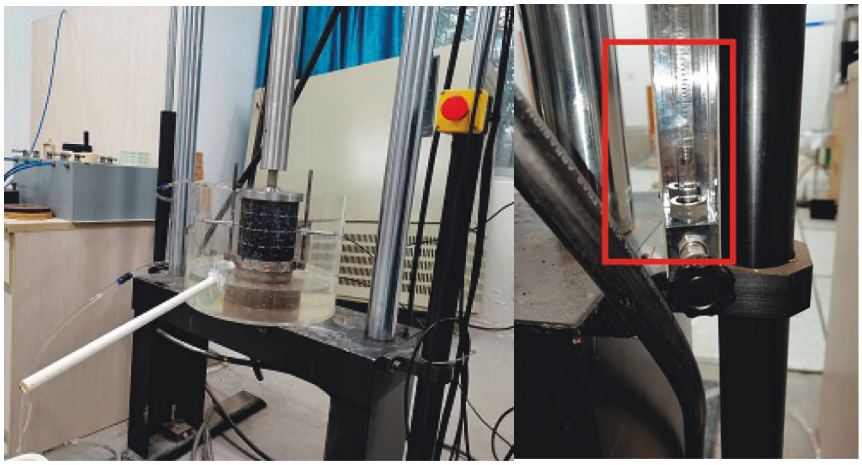

Figure 3: Seepage field-stress field coupling test.

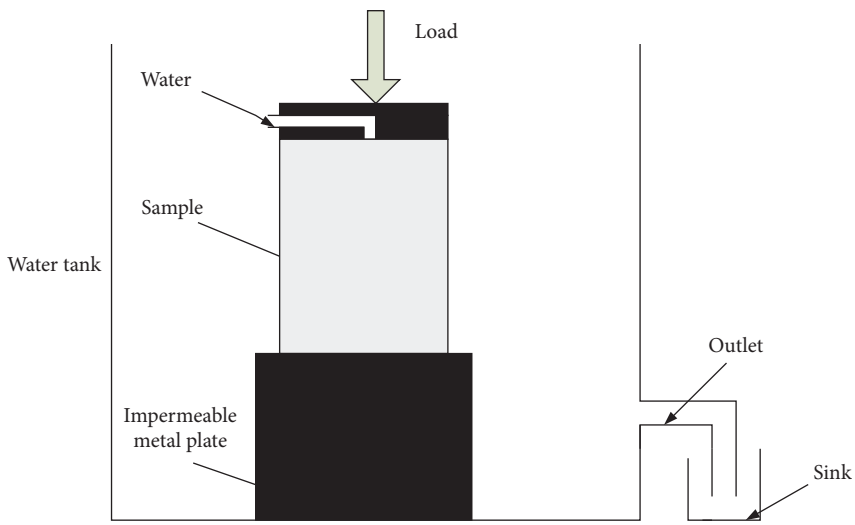

Figure 4: Schematic diagram of the seepage field-stress field coupling test.

average seepage velocity of water in the porous medium (m/s), and k is the hydraulic conductivity (m^2).

Therefore, it is necessary to convert k into a permeability coefficient K (m/s), as follows:

$$K = k\frac{\rho g}{\mu}. \tag{6}$$

According to Figure 5 and equation (6), equation (5) is changed to an expression of the head gradient:

$$-\frac{\Delta\phi}{\Delta X} = \frac{u}{K}. \tag{7}$$

When the effective porosity of the porous medium is large, it is generally considered that the seepage of water in the porous medium is non-Darcy flow and satisfies the Forchheimer equation, which can be expressed using either of the following forms [19, 20]:

$$-\frac{\partial P}{\Delta X} = \frac{\mu u}{k} + \beta\rho u^2, \tag{8}$$

$$-\frac{\partial\phi}{\Delta X} = \frac{u}{K} + \frac{\beta}{g}u^2, \tag{9}$$

where β is the Forchheimer coefficient (1/m). The meanings of the other parameters are the same as above.

The permeability coefficient (or hydraulic conductivity) of the compacted permeable asphalt mixture is obtained based on Figures 5 and 6, equations (1)–(9), and the following test steps:

(1) After the permeable asphalt mixture specimen underwent the repeated uniaxial compression test under seepage and stress field coupling, according to the non-Darcy flow permeability coefficient tester described above, the water drainage volume M at

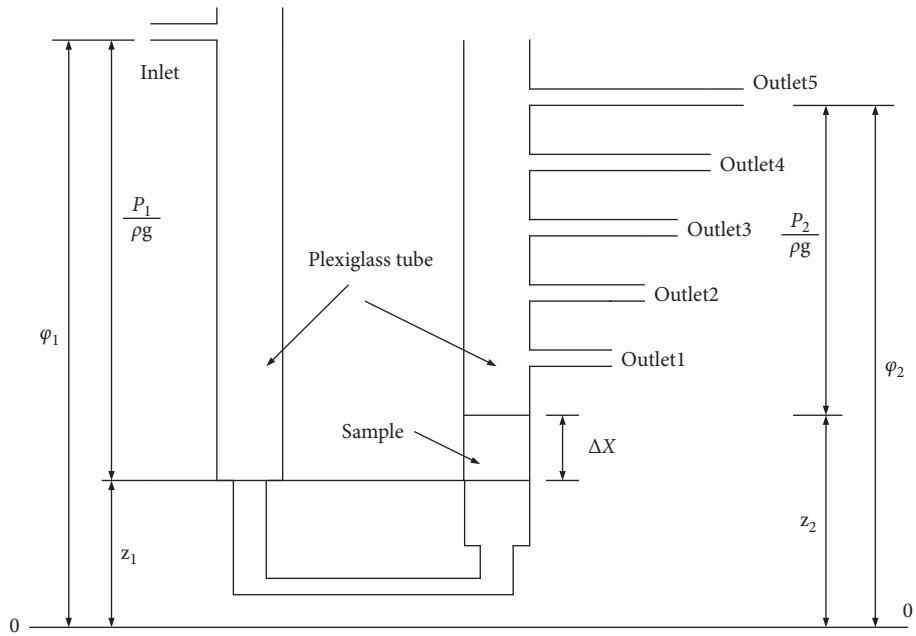

Figure 5: Schematic diagram of non-Darcy flow permeability coefficient tester.

Figure 6: Non-Darcy flow permeability coefficient tester for compacted PFC-13 specimen.

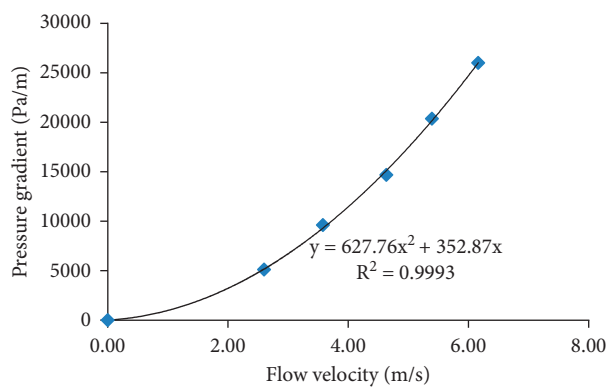

Figure 7: Flow velocity vs. water head gradient.

time t was measured five times. The maximum and minimum values among the five values were removed, whereupon the average value $\overline{M}$of the remaining three values was calculated.

(2) Q was calculated as follows:

$$Q = \frac{\overline{M}}{t}. \tag{10}$$

(3) The average seepage velocity was calculated using equation (3) or (4)

(4) The water pressure gradient was calculated

(5) The water outlet height was changed, which in turn changed the water pressure gradient

(6) According to steps (1)–(4), five groups of seepage velocities and their corresponding pressure gradients were obtained

(7) Based on equation (8) or (9), the above five sets of data were fitted with a one-variable quadratic equation, as shown in Figure 7

(8) Based on equation (8) or (9), the coefficients of the first-order and second-order terms of the one-variable quadratic fitting equation were converted into a k or K value and a β value.

Based on the fit shown in Figure 7, $\beta\rho = 627.76$ and $\mu/k = 352.87$. The β and k values were calculated according to the density and dynamic viscosity of water: β was 0.628 and k was 2.862×10^{-6}. Based on the k values and (6), k was transformed into K, and K was 27.801 m/s. The test procedure from Step (1) to Step (8) is shown in Figure 8.

From the non-Darcy flow permeability coefficient test, the relationship between the permeability coefficient and

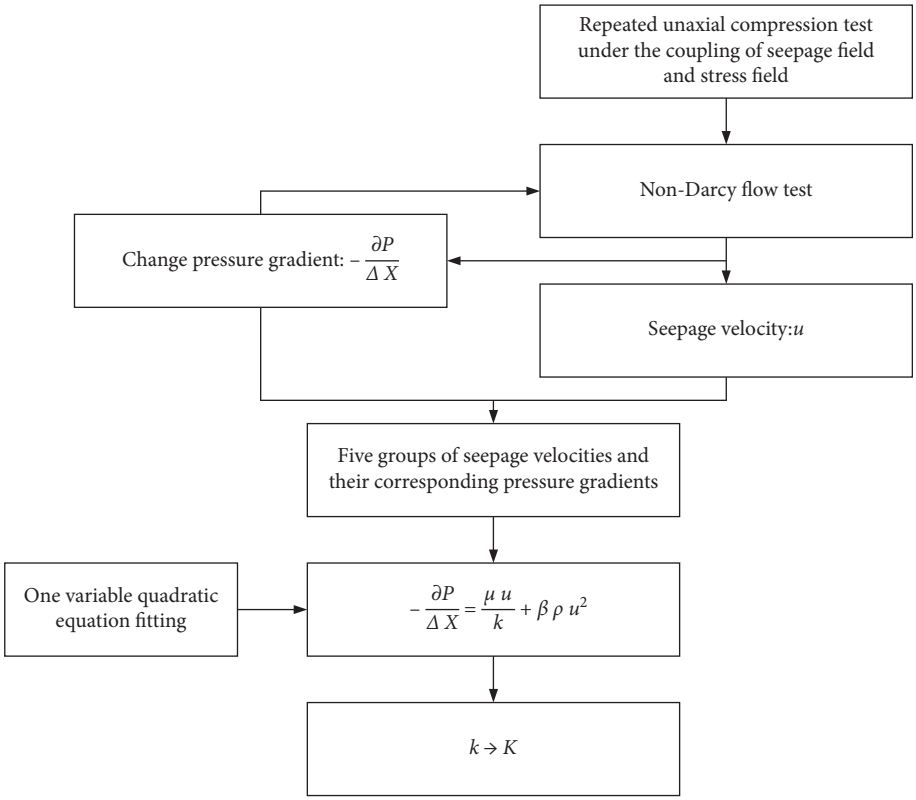

Figure 8: Test process of non-Darcy flow permeability coefficient.

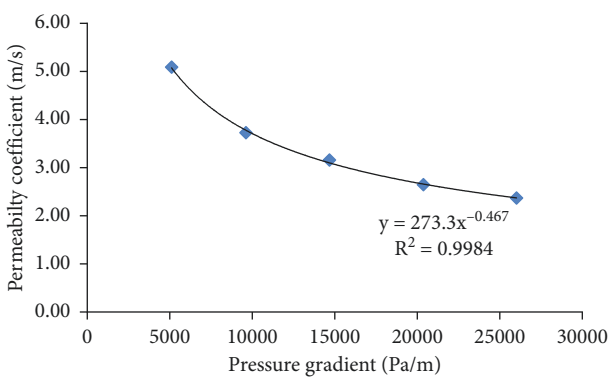

Figure 9: Permeability coefficient vs. pressure gradient.

Figure 10: PFC-13 specimens prepared with a gyratory compactor.

pressure gradient was determined, as shown in Figure 9. The water flow in the permeable asphalt mixture specimen was a typical non-Darcy flow, and the permeability coefficient had a nonlinear relationship with the pressure gradient.

6. Testing Plan

6.1. Preparation of PFC-13 Specimen. According to the combined aggregate gradation and the optimal asphalt-aggregate ratio of the PFC-13 mixture, PFC-13 specimens with 150 mm diameters and 150 mm heights were prepared with a gyratory compactor, as shown in Figure 10.

In this study, the vacuum sealing method was used to measure the bulk-specific densities of the PFC-13 specimens and to calculate the total air void and effective air void ratios, as shown in Figure 11. The results are shown in Table 7. The effective air void ratio was about 5% smaller than the total air void ratio, which fully indicated that there were partially closed pores in the compacted PFC-13 sample, which would not affect its permeability.

6.2. Test Load. The test load of this study was set as a contact pressure between a rubber tire and asphalt pavement of 700 kPa, i.e., a standard contact load. Under the action of the above three contact loads, the variation characteristics of the permeability of the compacted permeable asphalt mixture samples were studied. The load waveform was half a sine wave with a frequency of 10 Hz. After the PFC-13 specimens underwent repeated uniaxial compression under water and

Figure 11: Total air void and effective air void ratios determined using the vacuum sealing method.

Table 7: Total air void and effective air void ratios of PFC-13 specimens.

No.	Bulk-specific relative density	Theoretical maximum relative density	Total air voids (%)	Effective air voids (%)
1	1.971	2.450	19.6	14.6
2	1.911	2.450	22.0	18.5

load coupling, the total air void ratio, effective air void ratio, sample height, and permeability coefficient were measured.

7. Results and Discussion

In order to reduce the influence of water in the pores on the total air void ratio and especially on the effective air void ratio, after repeated uniaxial compression tests, the samples were first dried by fans. During the drying process, the water in the pores basically flowed out under the dual effects of self-weight and wind. In the process of drying, the sample mass was determined by weighing. If the weight difference between two consecutive times was less than 0.1%, it indicated that the water in the sample flowed out completely.

7.1. Effect of Seepage Field on Damage Factors. In order to compare the influence of the seepage field on the damage factor, the damage factor was calculated as follows:

$$H = \frac{h_0 - h_n}{h_0}, \tag{11}$$

where H is the damage factor, h_0 is the original height of the sample (mm), and h_n is the height of the sample after n cycles of repeated uniaxial compression testing (mm).

Repeated uniaxial compression tests were carried out on PFC-13 specimens under a nonseepage field and a seepage field. Based on (10), the damage factors were calculated, as shown in Figure 12. For the same number of repeated uniaxial compression cycles, namely, 2 million cycles, the damage factor was about 0.006 for the nonseepage field, but the damage factor was about 0.025 for the seepage field. The ratio of 0.025–0.006 was 4.2, indicating that the seepage field along with the stress field heavily accelerated the damage of the PFC-13 specimens.

7.2. Effect of Seepage Flow Field on Total Air Void and Effective Air Void Ratios. In order to eliminate the influence of the initial air voids on the number of repeated uniaxial compression cycles, the total air void and effective air void ratios were measured after each repeated uniaxial compression test and were divided by the initial total air void and effective air void ratios. The ratio of these two sets of data was used to express the change in voids. Then, the relationships between the ratios and the number of repeated uniaxial compression cycles are shown in Figures 13 and 14. It can be seen from Figure 13 that when the total air void ratio was 1%, the number of repeated uniaxial compression cycles for the nonseepage field was about 1.5 times that for the seepage field. It can be seen from Figure 14 that when the effective void ratio was about 1%, the number of repeated uniaxial compression cycles for the nonseepage field was about 1.3 times that of the seepage field.

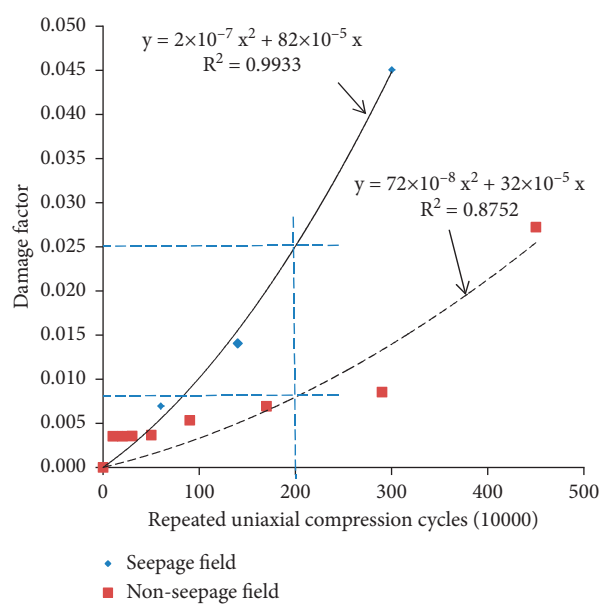

Figure 12: Relationship between the number of uniaxial loading cycles and the damage factor.

Therefore, under the coupled action of the seepage field and the stress field, the changes in total air void and effective

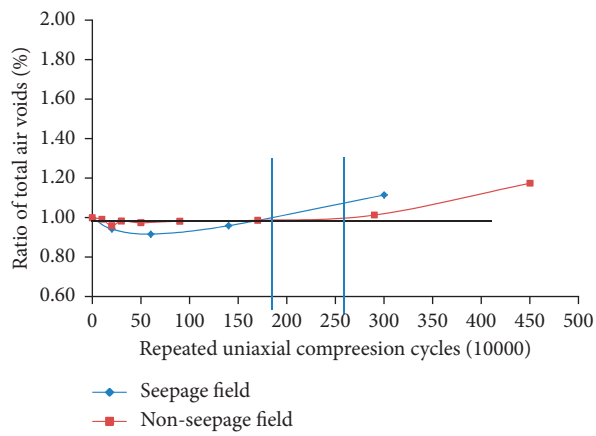

Figure 13: Relationship between repeated uniaxial compression cycles and ratio of total air voids.

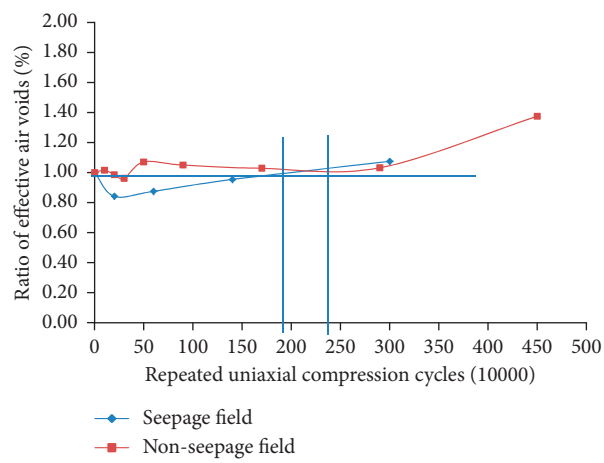

Figure 14: Relationship between repeated uniaxial compression cycles and ratio of effective air voids.

air void ratios of PFC-13 were accelerated. At the same time, the total air void and effective air void ratios decreased first and then increased with the increase in the number of repeated uniaxial compression cycles. This showed that the PFC-13 specimen was compacted first and then cracks appeared in the specimen. Then, changes in the displacement of the aggregates began to occur, and the specimen was damaged.

7.3. Effect of Seepage Field on Permeability Coefficient. Figure 15 shows the relationship between the number of repeated uniaxial compression cycles and the non-Darcy flow permeability coefficient. When the permeability coefficients were the same, the seepage field had a great impact on the number of repeated uniaxial compression cycles, and this effect was more significant with the increase in the number of repeated uniaxial compression cycles. When the permeability coefficient was 500 m/s, the number of repeated uniaxial compression cycles with the nonseepage field was about 1-2 times that with the seepage field. Therefore, the coupled effect of the seepage field and the stress field accelerated the water damage of the PFC-13 specimen.

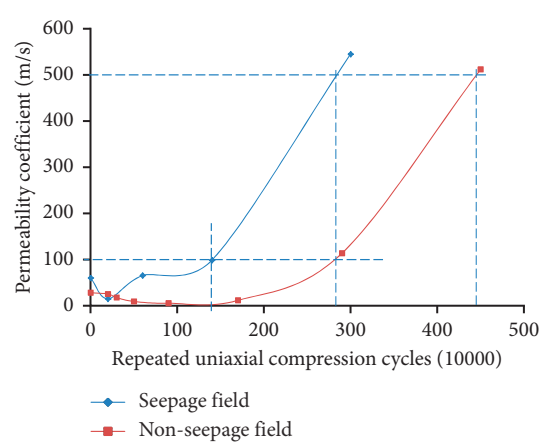

Figure 15: Relationship between repeated uniaxial compression cycles and permeability coefficient.

Furthermore, it was found that the non-Darcy flow permeability coefficient decreased first and then increased with the increase in the number of repeated uniaxial compression cycles, which fully showed that the PFC-13 specimen was further compacted first and then gradually

Table 8: Repeated uniaxial compression test results with non-seepage field.

Repeated uniaxial compression cycles (10000)	Total air voids (%)	Effective air voids (%)	Damage factor	Permeability coefficient (m/s)
450	23.0	20.1	0.0272	512.243
290	19.8	15.1	0.00855	113.884
170	19.3	15.0	0.00693	11.883
90	19.2	15.3	0.00535	5.525
50	19.1	15.6	0.00367	9.418
30	19.2	14.1	0.00356	17.828
20	18.8	14.4	0.00355	25.648
10	19.4	14.85	0.00355	—
0	19.6	14.6	0	28.339

Table 9: Repeated uniaxial compression test results with seepage field.

Repeated uniaxial compression cycles (10000)	Total air voids (%)	Effective air voids (%)	Damage factor	Permeability coefficient (m/s)
300	23.8	19.9	0.0456	545.256
140	20.5	17.7	0.0141	99.128
60	19.6	16.2	0.00698	65.716
20	20.2	15.6	0.00375	15.537
0	22.0	18.5	0	60.310

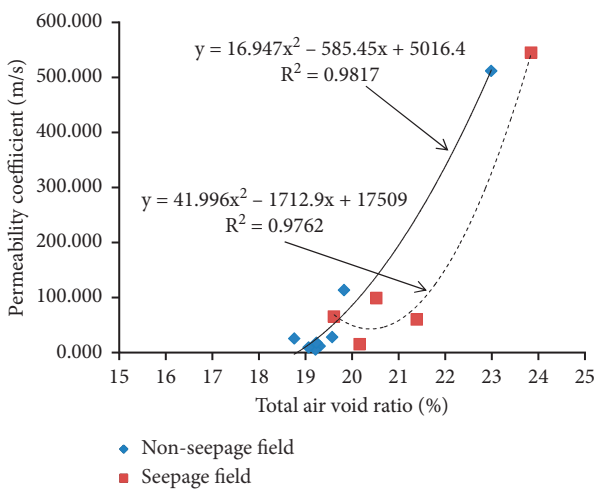

Figure 16: Relationship between total void ratio and non-Darcy flow permeability coefficient.

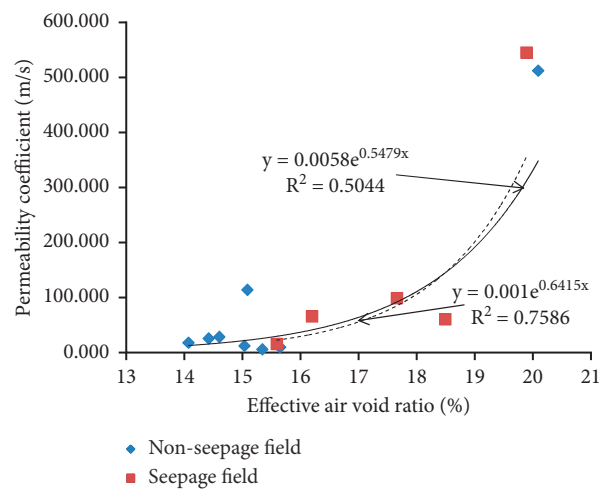

Figure 17: Relationship between effective void ratio and non-Darcy flow permeability coefficient.

developed cracks during the repeated uniaxial compression test.

7.4. Relationship between Non-Darcy Flow Permeability Coefficient and Air Voids. Curves relating the total air void and effective air void ratios to the non-Darcy flow permeability coefficient (Tables 8 and 9) are shown in Figures 16 and 17, respectively. According to Figure 16, the non-Darcy flow permeability coefficient followed a one-dimensional quadratic relation with the total air void percentage. When the total air void percentage exceeded 21.4%, the permeability coefficient increased sharply. Figure 17 shows that the correlation between the permeability coefficient and the effective air voids was adequate, which could be described by an exponential function. The overall variation trend was that the non-Darcy flow permeability coefficient increased with the increase in the effective air void ratio. Similarly, when the effective air void ratio was about 18.1%, the non-Darcy flow permeability coefficient increased significantly.

8. Conclusions

In this paper, a draindown loss test and power function fitting were used to determine the optimal asphalt-aggregate ratio of a PFC-13 mixture. The coupled action of water and a repeated compression load on PFC-13 specimens was examined. The vacuum sealing method was used to measure the total air void and effective air void ratios. A non-Darcy flow test device was made to measure the permeability coefficients of the PFC-13 specimens. It was found that the damage factor, total air void ratio, effective air void ratio, and permeability coefficient were influenced by the seepage and stress fields under repeated uniaxial compression conditions. The conclusions were as follows:

(1) Under the same number of repeated uniaxial compression cycles, namely, 2 million cycles, the damage factor for the seepage field was about 4.2 times that for the nonseepage field

(2) When the total air void ratio was 1%, the number of repeated uniaxial compression cycles for the specimen without the seepage field was about 1.5 times that of the specimen with the seepage field. When the effective void ratio was about 1%, the number of repeated uniaxial compression cycles of the specimen with the nonseepage field was about 1.3 times that of the sample with the seepage field.

(3) When the permeability coefficient was 500 m/s, the number of repeated uniaxial compression cycles for the specimen with the nonseepage field was about 1-2 times that of the specimen with the seepage field. Furthermore, the non-Darcy flow permeability coefficient decreased first and then increased with the increase in the number of repeated uniaxial compression cycles.

(4) When the total void ratio exceeded 21.4%, the permeability coefficient increased significantly. The effective void ratio was about 18.1%, and the permeability coefficient changed significantly. Therefore, the coupled effect of seepage and stress fields accelerated the water damage of the permeable asphalt pavement. In the permeable asphalt mixture, the water flow was non-Darcy flow.

In the future, after the coupling of the seepage and stress fields, the aggregate structure changes in permeable asphalt mixtures will be studied. The permeability properties and the crack evolutionary process will be explored under the coupled action of multiple factors, namely, seepage, stress, and temperature fields.

Data Availability

The data used to support the findings of this study are included within the article.

Conflicts of Interest

The authors declare that they have no conflicts of interest.

Authors' Contributions

The work presented herein was carried out in collaboration between all the authors. Zhang Xingmei was responsible for the study conception and design. Li Yaru was responsible for data collection and writing. Yang Datian was responsible for the analysis and interpretation of the data. All the authors reviewed the results and approved the final version of the manuscript.

Acknowledgments

This study was supported by the Chongqing Municipal Education Commission Foundation (KJQN201804001) and the Guangxi Science Research and Technology Development Plan Project (Guikegong1598009-11). The authors thank LetPub (https://www.letpub.com) for its linguistic assistance during the preparation of this manuscript.

Supplementary Materials

In the manuscript, the manuscript was copyedited for English language by LetPub (www.letpub.com), with regard to grammar, punctuation, spelling, and clarity. All of language editors are native English speakers with long-term experience in editing scientific and technical manuscripts. (*Supplementary Materials*)

References

[1] National Academies of Sciences, "Engineering, and medicine," *Constructionand Maintenance Practices for Permeable Friction Courses*, TheNational Academies Press, Washington, DC, 2009.

[2] Ministry of Communications of the People's Republic of China and JTG E20-2011, *Technical Specification for Construction of Highway Asphalt Pavement*China Communications Press Co. LTD., Beijing, China, 2005.

[3] Ministry of Communications of the People's Republic of China and JTG E20-2011, *Standard Test Methods of Bitumen and Bituminous Mixtures for Highway Engineering*China Communications Press Co. LTD., Beijing, China, 2011.

[4] A. Eduardo Alvarez, A. Epps-Martin, C. Estakhri, and R. Izzo, "Evaluation of Durability tests for permeable friction course mixtures," *International Journal of Pavement Engineering*, vol. 11, no. 1, pp. 49–60, 2010.

[5] T. Aashto, *324 Standard Method of Test for Hamburg Wheel-Track Testing of Compacted Asphalt Mixtures*, p. 324, AASHTO Designation, Washington, D.C, 2019.

[6] L. Poulikakos, S. Takahashi, and M. N. Partl, "Coaxial shear test and wheel tracking tests for determining porous asphalt mechanical properties," *Road Materials and Pavement Design*, vol. 8, no. 3, pp. 579–594, 2007.

[7] W. Huang, H. Yu, Yi Lin et al., "Energy analysis for evaluating durability of porous asphalt mixture," *Construction and Building Materials*, vol. 326, no. 4, Article ID 126819, 2022.

[8] D. Yang and Q. Zhou, "Effect of immersion conditions on fatigue life of asphalt concrete," *Road construction machinery and construction mechanization*, vol. 35, no. 3, pp. 54–59+64, 2018.

[9] N. Kringos, T. Scarpas, C. Kasbergen, and P. Selvadurai, "Modelling of combined physical mechanical moisture-induced damage in asphaltic mixes, Part 1: governing processes and formulations," *International Journal of Pavement Engineering*, vol. 9, no. 2, pp. 115–128, 2008.

[10] C. D. Si, E. L. Chen, Z. You, R. Zhang, P. Qiao, and Y. Feng, "Dynamic response of temperature-seepage-stress coupling in asphalt pavement," *Construction and Building Materials*, vol. 211, pp. 824–836, 2019.

[11] Y. M. Ding and H. Wang, "Evaluation of hydroplaning risk of permeable friction course using 3-D grooved tire-water-pavement interaction model," *Int. Assoc. Chin. Infrastruct. Professionals*, vol. 2672, 2018.

[12] Y. Sun, R. Guo, X. Wang, and X. Ning, "Dynamic response characteristics of permeable asphalt pavement based on unsaturated seepage," *International Journal of Transportation Science and Technology*, vol. 8, no. 4, pp. 403–417, 2019.

[13] C. Si, C. Si, F. Yang, and Y. Wang, "Finite element analysis of asphalt pavement on account of stress-seepage coupling field," *Metallurgical and Mining Industry*, vol. 6, pp. 259–266, 2015.

[14] Ministry of Communications of the People's Republic of China and JT/T 860.2-2013, *Modifier for Asphalt Mixture Part 2: High Viscosity Additive*China Communications Press CO. LTD., Beijing, China, 2013.

[15] Chongqing Municipal Commission of Municipal and Rural Construction and DBJ50/T-241-2016, *Technical Specification for Porous Asphalt Pavement*, Chongqing Municipal Commission of Municipal and Rural Construction, Chongqing, China, 2016.

[16] I. Tsvankin, "Handbook of geophysical exploration," *Seismic Exploration*, vol. 31, no. 2, pp. 219–293, 2001.

[17] Q. Li, Q. Zhu, J. Zheng, K. Liao, and G. Yang, "Soil moisture response to rainfall in forestland and vegetable plot in taihu lake basin, China," *Chinese Geographical Science*, vol. 25, no. 4, pp. 426–437, 2015.

[18] B. Jacob, *Dynamics of Fluids in Porous media*, America Elsevier Publishing Company, Inc, New York, NY, 1972.

[19] Z. Zeng and G. Reid, "A Criterion for Non-Darcy Flow in Porous," *Media Transport in Porous Media*, vol. 63, no. 1, pp. 57–69, 2006.

[20] J. S. Wu, H. U. DeZhi, L. I. Wenjun, and C. A. I. Xin, "A review on non-Darcy flow-forcheimer equation, hydraulic radius model, fractal model and experiment," *Fractals*, vol. 24, no. No. 2, p. 13, Article ID 1630001, 2016.